WILEY-VCH

Semiconducting Small Molecules as Active Materials for p-Type Accumulation mode Organic Electrochemical Transistors

*Zachary S. Parr, Reem B. Rashid, Bryan D. Paulsen, Benjamin Poggi, Ellasia Tan, Mark Freeley, Matteo Palma, Isaac Abrahams, Jonathan Rivnay, and Christian B. Nielsen**

Z. S. Parr, B. Poggi, E. Tan, M. Freeley, Dr. M. Palma, Dr. I. Abrahams, Dr. C. B. Nielsen
Materials Research Institute and School of Biological and Chemical Sciences, Queen Mary University of London, Mile End Road, London, E1 4NS, UK
E-mail: c.b.nielsen@qmul.ac.uk

R. B. Rashid, Dr. B. D. Paulsen, Prof. J. Rivnay
Department of Biomedical Engineering, Northwestern University, Evanston, Illinois, 60202, USA

Keywords: π-conjugated small molecules, organic electrochemical transistors, mixed ionic-electronic conduction

A series of semiconducting small molecules with bithiophene or bis-3,4-ethylenedioxy-thiophene cores are designed and synthesised. The molecules display stable reversible oxidation in solution and can be reversibly oxidized in the solid state with aqueous electrolyte when functionalized with polar triethylene glycol side chains. Evidence of promising ion injection properties observed with cyclic voltammetry is complemented by strong electrochromism probed by spectroelectrochemistry. The effect of blending these molecules with high molecular weight polyethylene oxide is found to improve both ion injection and thin film stability. The molecules and their corresponding polyethylene oxide blends are investigated as the active layers in organic electrochemical transistors (OECTs). For the most promising molecule:polymer blend (P4E4:PEO) p-type accumulation mode OECTs with μA drain currents, μS peak transconductances and a μC* figure-of-merit value of 0.81 F V^{-1} cm^{-1} s^{-1} are obtained.

1. Introduction

Organic electrochemical transistors (OECTs), as depicted schematically in **Figure 1**, have been widely explored for interfacing organic electronics with biologically and medically

relevant systems.[1,2] The burgeoning field of organic bioelectronics has seen OECTs employed in a wide range of applications from neural interface devices for epileptogenic centers,[3] to biological analyte detection,[4–7] cardiac monitoring,[8] whole cell interface monitoring,[9,10] pH sensing,[11] in ion pumps,[12] and electronic plants.[13] While OECTs traditionally have comprised the conducting polymer mixture poly(3,4-ethylenedioxy-thiophene):polystyrene sulfonate (PEDOT:PSS), semiconducting polymers have more recently been implemented as the active material in OECTs. The electrochemical gating of the OECT necessitates mixed conduction of electronic and ionic charges in the transistor channel. To facilitate this, traditional semiconducting polymers have been modified with polar side chains and in particular oligoether side chains.[14,15] This development has enabled the community to start elucidating structure property relationships in ionic-electronic mixed conductors.[16–18]

The potential advantages of small molecules in organic electronics have been well documented for organic field-effect transistors (OFETs) with very high charge carrier mobilities observed for instance for C_8-BTBT.[19]

A number of biological sensing devices based on small molecule semiconductors have been reported including: pentacene as an antibody sensor,[20] a phosphonate sensor,[21] and as chiral small molecule sensors.[22] These devices have been based on thin film OFET configurations and not an OECT configuration with volumetric operation of the semiconductor. As such, discrete conjugated molecules capable of mixed ionic and electronic conduction could potentially provide a new design platform for active materials for OECT applications. It could furthermore provide an alternative route to investigating structure-property relations for organic mixed ionic-electronic conductors.

In this work, 5,5'-bis(4-hexylphenyl)-2,2'-bithiophene (PTTP-C_6), a well-known small molecule transistor material with a hole mobility around 0.1 $cm^2 v^{-1} s^{-1}$,[23] is explored as a

simple and easily modifiable starting point for the design of a proof-of-concept small molecule mixed ionic-electronic conductor for OECT applications. We initially substituted the peripheral hexyl chains with triethylene glycol chains to allow for aqueous ion penetration in a thin film. Subsequently, we increased the electron-rich character of the molecule by introducing 3,4-ethylenedioxythiophene (EDOT) units and further extended the molecule length to improve π-stacking and intermolecular charge transport. Following this approach, an OECT with a small molecule active layer is demonstrated, while improved device performance is achieved when blending the small molecule with high molecular weight polyethylene oxide.

2. Results and Discussion

2.1. Synthesis and Characterisation

The molecules discussed herein were synthesised according to **Scheme 1**; full details of synthesis are available in the Supporting Information (SI Section 2.0). Briefly, the triethylene glycol side chain was synthesised via functionalisation of 2-(2-(2-methoxyethoxy)-ethoxy)ethan-1-ol with 4-methylbenzenesulfonyl chloride in basic conditions in tetrahydrofuran/water at room temperature to afford 2-(2-(2-methoxyethoxy)ethoxy)ethyl 4-methylbenzenesulfonate (**1**) in 67% yield. Compound **1** was subsequently reacted with 4-bromophenol or 4'-bromo-(1,1'-biphenyl)-4-ol to afford 1-bromo-4-(2-(2-(2-methoxyethoxy)-ethoxy)ethoxy)benzene (62% yield) (**2**) and 4-bromo-4'-(2-(2-(2-methoxyethoxy)ethoxy)-ethoxy)-1,1'-biphenyl (85% yield) (**3**), respectively. Compound **2** served as the aryl halide component for a Stille coupling reaction with 5,5'-bis(trimethylstannyl)-2,2'-bithiophene to afford **PTTP** as an orange powder in 53% yield. In order to access the bi-EDOT derivative **P2E2**, we employed a modified method of direct arylation reported for EDOT oligomers and polymers as a simple, scalable and greener method of synthesizing the target molecules.[24,25] 2,2',3,3'-Tetrahydro-5,5'-bithieno[3,4-b][1,4]dioxine (bi-EDOT) was reacted with two

equivalents of aryl halide **2** in dimethylformamide with potassium carbonate and tetrabutyl-ammonium bromide, pivalic acid and palladium (II) acetate to afford **P2E2** in a reasonable yield of 56%. Reacting an excess of bi-EDOT with aryl halide **3** under the same conditions afforded compound **5** in 63% yield. Compound **5** was subsequently dimerized via oxidative coupling with ferric chloride to afford **P4E4** as a dark red solid in 95% yield. The final molecules showed high thermal stability with 5% mass loss observed by thermogravimetric analysis at 302 °C for **PTTP-C$_6$**, 358 °C for **PTTP**, 373 °C for **P2E2** and 343 °C for **P4E4** (SI Section 3.0).

2.2. Electrochemical Characterisation

The molecules were initially characterized by cyclic voltammetry (CV) in dichloromethane (DCM) solution with results summarized in **Table 1** and SI Section 5.0. Reversible oxidation events were observed for **PTTP-C$_6$** for formation of the radical cation and dication with half-wave potentials ($E_{1/2}$) of 0.51 V and 1.01 V respectively versus ferrocene/ferrocenium (Fc/Fc^+), whereas **PTTP** exhibited slightly lower half-wave potentials of 0.39 V and 0.75 V. The reduced half-wave potentials of **PTTP** are likely a result of the mesomeric effect of direct attachment of oxygen on the phenyl ring, increasing electron density on the conjugated backbone. For **P2E2**, clearly resolved first and second oxidation events with $E_{1/2}$ values of 0.04 V and 0.50 V for cation and dication formation respectively are observed. Compared to **PTTP**, the electron-rich EDOT units lower the half-wave potentials of **P2E2**. Similarly, **P4E4** has further reduced half-wave potentials with two less well resolved oxidation events with $E_{1/2}$ values of 0.01 V and 0.23 V. The lower half-wave potential of **P4E4** compared to that of **P2E2** for the second oxidation event to the dication is attributed to the increasingly electron-rich core combined with a longer conjugation length, resulting in lower coulombic repulsion of charges on the backbone.

Electrochemical conditions more relevant to OECT operation were probed by solid state CV in aqueous electrolyte with resulting voltammograms depicted in **Figure 2** and data

summarized in Table 1. Unsurprisingly, the hydrophobic **PTTP-C$_6$** could not be oxidized as the resistance to ion injection is too high to allow oxidation below the electrolysis potential of water. Introduction of the triethylene glycol chains in **PTTP** allows ion injection with the film showing a non-reversible oxidation event with a high onset of oxidation of 0.93 V versus Ag/Ag^+. **P2E2** exhibited a well resolved reversible oxidation event with $E_{1/2}$ of 0.46 V and an onset potential of 0.34 V. Compared to **P2E2**, the longer and more electron-rich **P4E4** showed a significantly lower onset of oxidation of 0.22 V with the first half-wave potential observed at 0.10 V as well as a second half-wave potential at 0.73 V for the oxidation event from radical cation to dication. Following a strong initial charge injection or memory peak previously noted for conducting polymers,[26] **P2E2** and **P4E4** films exhibited stable reversible redox behavior over many CV scans (SI Section 5.5).

To improve charge injection into the film and overcome the low viscosity of small molecule solutions, films with 10 wt% high molecular weight polyethylene oxide (PEO) (M_v 900 KDa) were also investigated.[27],[28] The molecule:PEO blend solutions were drop cast onto the glassy carbon electrodes under the same conditions as for the neat molecule-based films. The **P2E2**:PEO blend (Figure 2b) exhibited an $E_{1/2}$ value of 0.46 V and an onset potential of 0.34 V for the for the first oxidation event which is identical to what was observed for the neat molecule thin film. Slightly improved long-term electrochemical cycling stability was observed for the **P2E2**:PEO blend compared to the neat electroactive material (SI Section 5.6). For the **P4E4**:PEO blend, we likewise observed nearly identical first and second half-wave potentials to what was observed for the neat **P4E4** film. We do however note upon blending with PEO that the first onset of oxidation was lowered by approximately 0.1 V concurrent with a significant increase in current density (Figure 2c), suggesting more effective ion injection in the blend film. Introduction of PEO had no effect on the aqueous switching of **PTTP-C$_6$** and **PTTP** thin films (SI Section 5.9 and 5.10). From variable scan rate CV experiments, a linear relationship between peak current and the square-root of the

scan rate was observed for both neat **P2E2** and **P4E4** films and their PEO blends (SI section 5.11).[29] This indicates a diffusion-controlled charge injection process in all four cases with extracted ionic diffusion coefficients plotted in Figure 2d. An increase of ionic diffusion coefficient across the series **P2E2** < **P2E2**:PEO < **P4E4** < **P4E4**:PEO suggests that **P4E4**:PEO has the most favorable ion injection under these conditions. The measured ionic diffusion coefficients are higher than those of partially glycolated polythiophenes and the value for the **P4E4**:PEO blend is only marginally lower than that of the high-performing OECT material p(g2T-TT).[30]

2.3. Optical Characterisation

Optical characterisation of solutions and films of the molecules was carried out by UV-Vis-nIR spectroscopy as depicted in **Figure 3** and SI Section 5.1 and 5.2. A gradual red shift in absorption maximum (λ_{max}) was observed across the series going from **PTTP** (380 nm) to **P2E2** (401 nm) and **P4E4** (480 nm) with vibronic features observed for **P2E2** and **P4E4** owing to the planarising intramolecular S-O interactions. The thin film spectra exhibited the same trend in λ_{max} as the solutions with **P4E4** having a broadened and slightly red-shifted spectrum with λ_{max} 485 nm and additional features around 462 nm and 532 nm. **P2E2** thin films exhibited a significant red shift over the solution phase by 51 nm with λ_{max} 452 nm and significant vibronic shoulders at 284 nm and 420 nm. **PTTP** exhibited a slight blue shift in thin film over the solution phase, suggesting poorer packing or H-aggregates in the solid state with λ_{max} of 358 nm. Optical band gaps were calculated from the onset of absorption in the thin films and found to be 2.88 eV, 2.66 eV and 2.13 eV for **PTTP**, **P2E2** and **P4E4** respectively.

Thin film spectroelectrochemistry was employed to probe the formation and stability of oxidized species in aqueous electrolyte. For **P2E2**, we observed a gradual increase of the radical cation bands with absorption maxima at 630 nm and 1072 nm with concurrent bleaching of the π-π* transition at 401 nm for voltages between 0.1 V and 0.5 V (Figure 3c).

Subsequently, at increasing voltages, a band attributed to the dication **P2E2**$_2^{2+}$ with absorption maximum at 934 nm was observed.[31] The film could subsequently be reduced to the neutral state with around 50% loss of absorbance ascribed to degradation and partial film delamination. The **P2E2**:PEO film (Figure 3d) behaved similarly with formation of the radical cation (λ_{max} values at 628 and 1062 nm) and subsequently the dication (λ_{max} 928 nm) combined with quenching of the π-π* transition. Compared to neat **P2E2**, the PEO-containing film degraded less during electrochemical cycling and could be reduced back to around 75% of initial absorbance. For **P4E4**, growth of two broad radical cation absorption features was observed with absorption maxima at 620 nm and 1018 nm for the neat film and at 600 nm and 1018 nm for the **P4E4**:PEO blend (Figure 3e-f). We note that the **P4E4** radical cation appear to form at slightly lower potential in the blend (~0.4 V) than in the neat film (~0.5 V), most likely due to the faster ion diffusion in the blend (Figure 2d). The **P4E4** dication afforded a peak with λ_{max} at 810 nm and 804 nm, respectively, for the neat and PEO-containing film. Both the neat **P4E4** and the blend film could be reduced back to neutral with retention of 75% of the initial absorption.

2.4. Physical Properties

Using the B3LYP density functional theory (DFT) method with 6-311++g (d,p) basis set using the SCRF model, we calculated the frontier orbital energies as well as optimized geometries. The DFT data is in good agreement with the experimentally observed narrowing of the optical band gap and decrease in the ionisation potential when going from **PTTP** to **P2E2** and to **P4E4** (SI Section 8.0). The oxygen atoms on the EDOT ethylene bridge have a well-known dipolar interaction with sulfur atoms of neighboring thiophene rings.[32] The DFT calculations corroborate these planarising interactions with **P2E2** and **P4E4** having highly coplanar energy-minimized conformations.

A crystal structure for **P2E2** was obtained from single crystals grown via anti solvent precipitation (CCDC deposition Number 1944170), (SI Section 9.1). In the crystal, **P2E2**

exhibited a completely planar backbone with an S-C-C-S dihedral angle of 0 º as a result of the S-O planarising interaction in good agreement with the DFT data. The torsion angle was 1.68 º for the S-C-C-C dihedral (phenyl-EDOT linkage), which is significantly more coplanar than predicted by DFT, most likely due to intermolecular interactions not accounted for in the gas phase DFT. Despite this high degree of backbone co-planarity, the crystal packing revealed a preference for **P2E2** to pack in a staggered arrangement as seen in **Figure 4**. Molecules are slipped in both *x* and *y* direction with respect to the previous molecule enforcing an edge to face structure preventing effective π-overlap (Figure 4a). The layers of molecules are packed at an angle of 65 º with respect to plane of the π-conjugated backbone which favors packing of peripheral side chains further discouraging π-overlap.

In order to assess the microstructure of neat and PEO-blended films of **P2E2** and **P4E4**, we carried out grazing incident wide angle x-ray diffraction scattering (GIWAXS) (Figure 4c-f). The 2-D GIWAXS patterns for **P2E2** neat and blended films reveal many discrete spots consistent with an oriented polycrystalline film (SI Section 9.2). Qualitatively, PEO containing **P2E2** films took on a marginally more isotropic ordering indicated by the subtle smearing out of the scattering peaks. In contrast, the neat film of **P4E4** scatters much more similarly to a semi-crystalline thin film. **P4E4** displays a strong lamellar like out-of-plane scattering peak at low q_z (~0.3 $Å^{-1}$) and a broad π-stack like peak at higher q_z (~1.55 $Å^{-1}$). The calculated lamellar-like d-spacing of 21 Å, is much shorter than the conjugated core of the molecule (ca. ~30 Å), much less the entire molecule including peripheral triethylene glycol chains. If this is in fact a lamellar like scattering, this implies a significant tilt to the stacking of the conjugated molecular core, which is supported by the out of plane π-stacking which shows a maximum approximately ±27° with respect to the q_z direction. Also observed were two distinct in-plane scattering peaks. A strong peak with weak second order at ~0.45 and 0.91 $Å^{-1}$, respectively, matches the interlayer d-spacing (~14 Å) of EDOT based thin films. A second strong in-plane peak at ~0.8 $Å^{-1}$ is potentially due to interchain spacing of the

end-capped triethylene glycol chains. Overall, these data are interpreted as indicating a tilted end-on orientation of **P4E4** molecules. When blended with PEO, the out-of-plane lamellar-like scatter shifts to lower q_z (~0.26 $Å^{-1}$), effectively a ~4.5 Å lamellar expansion to ~25.5 Å. Further, a new out-of-plane peak appeared at similar q to the in-plane peak attributed to the interlayer spacing. This implies the presence of a new edge-on scattering population. While the in-plane peak positions remain the same in the PEO blended films, the relative peak intensities of the two major peaks were inverted.

Atomic force microscopy (SI 10.0) was carried out on thin films of the neat molecules and their PEO blends. For **PTTP**, **P2E2**, and **P4E4**, continuous films were obtained with the smoother films obtained for **P2E2** with negligible difference between neat and blended films and mean surface roughness (R_a) values of 2.21 nm and 2.14 nm respectively. **P4E4** exhibited a rougher film with smaller crystallites than **P2E2**. The **P4E4**:PEO blend was also slightly rougher than the **P2E2** film. The increased roughness is likely as a result of more rapid nucleation due to the lower solubility of **P4E4**, with R_a values of 6.31 nm and 8.36 nm for neat and blended films, respectively.

2.5 Transistor Characterisation

P2E2 and **P4E4**, which both exhibited good electrochromic responses, were tested as the active material with and without PEO in organic electrochemical transistors according to previously reported procedures.[18,25] An aqueous NaCl electrolyte was dropped onto the device, an Ag/AgCl gate electrode was submerged in the electrolyte and the device was cycled three times before measurement to ensure stable recordings. Representative output and transfer curves can be seen in **Figure 5** and in SI Section 10.0. Initially, using neat **P2E2** as the active layer, we observed no current across a number of devices and different spin-coating conditions despite promising electrochromism in aqueous electrolyte. We attribute the poor performance to the staggered crystal packing in the solid state where molecules exhibit minimal π-stacking and therefore negligible electronic charge transport. When blending **P2E2**

with 10 wt% high molecular weight PEO, a device which exhibited a threshold voltage V_t of –0.28 V and a peak drain current of 6 nA was obtained (Figure 5a-b); the transconductance (g_m) could not be reliably extracted.

For OECTs fabricated with neat **P4E4** as the active material, we observed a turn on for the devices and a moderate nanoamp drain current over three devices with an on/off ratio of 10^1 (SI Section 11.1). The devices showed some hysteresis which could be mitigated by cycling of the devices and a slower sweep rate. We extracted a peak transconductance, g_m, of 0.14 μS at a gate voltage of –0.65 V averaged across three devices, representing to the best of our knowledge the first p-type small molecule based OECT. The most promising results were obtained from a blend of **P4E4** and 10 wt% PEO (Figure 5c-d). The devices were measured to have an average peak transconductance of 0.65 μS at a gate voltage of –0.47 V and on/off ratios around 10^2 for an average device thickness of 31 nm. The μC^* product, considered a good materials figure-of-merit for organic mixed ionic-electronic conductors, was found to be 0.81 F V^{-1} cm^{-1} s^{-1} in the saturation regime for **P4E4**:PEO while the inferior performance of the neat **P4E4**-based device prevented a reliable extraction of the μC^* product in that case.[18] Consistent with the CV and spectroelectrochemistry data, the OECTs with the PEO blend turned on at lower bias (V_t of –0.15 V) than the neat **P4E4**-based devices (V_t of –0.32 V) while considerably lower hysteresis was also observed for the PEO-containing active layer. The relatively low currents observed for both neat **P4E4** and its PEO blend made it difficult to extract the OECT charge carrier mobility with confidence and decoupling of the μC^* product is consequently the subject of further investigations.

3. Conclusion

Given their often-excellent electronic charge transport properties, with mobilities exceeding those of semiconducting polymers, combined ease of synthesis and modular construction, small molecules have been widely used as active materials in organic

electronics. We have shown here that mixed ionic-electronic conduction can also be facilitated in small molecules through molecular design. This has resulted in the first p-type small molecule OECT material, namely **P4E4**, to complement the rapidly expanding library of p- and n-type mixed conduction materials.[33,34] A μC* product, widely adopted as one of the main figures-of-merit for OECTs, of 0.81 F V^{-1} cm^{-1} s^{-1} was achieved for **P4E4** with 10 wt% high molecular weight PEO. Although lower than what has been reported for the best performing p-type OECT materials, this value is comparable to the μC* product for p(gNDI-g2T), a glycolated naphthalene diimide based n-type polymer, and aforementioned partially glycolated polythiophene based p-type materials.[18,30,35]

From a molecular design point of view, in order to explore the concept of mixed ionic-electronic conduction in small molecules, we have synthesised a series of small molecules based on thiophene or more electron-rich EDOT cores with glycolated phenyl flanking groups. For the small molecules comprising electron-rich EDOT cores and peripheral oligoether side chains, we have shown very efficient charge injection from aqueous environment with stable electrochemical cycling in the solid state and low onset potentials well below the potential for water electrolysis. By thin film spectroelectrochemistry, facile formation of radical cation and dication species was evidenced by strong electrochromic responses at low potential with an aqueous supporting electrolyte in both neat molecule and PEO blends. Despite charge injection being observed for **P2E2** films, no working OECTs were obtained, likely as a result of the polycrystalline nature of the film with inefficient π-stacking. Conversely, for neat **P4E4** films, we measured ion injection as well as moderate OECT transconductances and on/off ratios. Upon blending with high molecular weight PEO, we obtained a functioning device for **P2E2** with moderate nanoamp drain current, while much better performance was achieved with **P4E4** affording an OECT threshold voltage of –0.15 V and a peak transconductance value of 0.65 μS at a gate voltage of –0.47 V. We attribute the

more efficient charge transport in **P4E4** compared to **P2E2** to its semi-crystalline structure, which should be more tolerant to ion intercalation necessary for OECT operation.

With further optimisation, and better understanding of important parameters such as charge carrier mobility and ionic mobility, we envision small molecules being good candidates for new mixed ionic-electronic conduction materials and an ideal platform for elucidating in much greater detail the intricate structure-property relations associated with mixed conduction.

[CCDC 1944170 contains the supplementary crystallographic data for this paper. These data can be obtained free of charge from The Cambridge Crystallographic Data Centre via www.ccdc.cam.ac.uk/data_request/cif.]

Supporting Information
Supporting Information is available from the Wiley Online Library or from the author.

Acknowledgements
B.D.P. and J.R. gratefully acknowledge support from the National Science Foundation Grant No. NSF DMR-1751308. Z.S.P. and C.B.N. gratefully acknowledge support from the Academy of Medical Sciences & Wellcome Trust (SBF002/1158) and the Materials Research Institute. The authors thank Joseph Strzalka and Qingteng Zhang for beam line assistance and Dr Roberto Buccafusca for assistance with mass spectrometry analysis. This research used resources of the Advanced Photon Source, a U.S. Department of Energy (DOE) Office of Science User Facility operated for the DOE Office of Science by Argonne National Laboratory under Contract No. DE-AC02-06CH11357. This work utilized Northwestern University Micro/Nano Fabrication Facility (NUFAB), which is partially supported by Soft and Hybrid Nanotechnology Experimental (SHyNE) Resource (NSF ECCS-1542205), the Materials Research Science and Engineering Center (NSF DMR-1720139), the State of Illinois, and Northwestern University.

Received: ((will be filled in by the editorial staff))
Revised: ((will be filled in by the editorial staff))
Published online: ((will be filled in by the editorial staff))

References

[1] X. Strakosas, M. Bongo, R. M. Owens, *J. Appl. Polym. Sci.* **2015**, *132*, 41735.

[2] J. Borges-González, C. J. Kousseff, C. B. Nielsen, *J. Mater. Chem. C* **2019**, *7*, 1111.

[3] D. Khodagholy, T. Doublet, P. Quilichini, M. Gurfinkel, P. Leleux, A. Ghestem, E. Ismailova, T. Hervé, S. Sanaur, C. Bernard, G. G. Malliaras, *Nat. Commun.* **2013**, *4*, 1575.

[4] M. E. Welch, T. Doublet, C. Bernard, G. G. Malliaras, C. K. Ober, *J. Polym. Sci. Part A Polym. Chem.* **2015**, *53*, 372.

[5] X. Qing, Y. Wang, Y. Zhang, X. Ding, W. Zhong, D. Wang, W. Wang, Q. Liu, K. Liu, M. Li, Z. Lu, *ACS Appl. Mater. Interfaces* **2019**, *11*, 13105.

[6] M. Berto, C. Diacci, L. Theuer, M. Di Lauro, D. T. Simon, M. Berggren, F. Biscarini, V. Beni, C. A. Bortolotti, *Flex. Print. Electron.* **2018**, *3*, 024001.

[7] S. Y. Yang, J. A. DeFranco, Y. A. Sylvester, T. J. Gobert, D. J. Macaya, R. M. Owens, G. G. Malliaras, *Lab Chip* **2009**, *9*, 704.

[8] X. Gu, S. Y. Yeung, A. Chadda, E. N. Y. Poon, K. R. Boheler, I. M. Hsing, *Adv. Biosyst.* **2019**, *3*, 1800248.

[9] M. P. Ferro, L. Leclerc, M. Sleiman, B. Marchiori, J. Pourchez, R. M. Owens, M. Ramuz, *Adv. Biosyst.* **2019**, *3*, 1800249.

[10] L. H. Jimison, S. A. Tria, D. Khodagholy, M. Gurfinkel, E. Lanzarini, A. Hama, G. G. Malliaras, R. M. Owens, *Adv. Mater.* **2012**, *24*, 5919.

[11] F. Mariani, I. Gualandi, M. Tessarolo, B. Fraboni, E. Scavetta, *ACS Appl. Mater. Interfaces* **2018**, *10*, 22474.

[12] A. Williamson, J. Rivnay, L. Kergoat, A. Jonsson, S. Inal, I. Uguz, M. Ferro, A. Ivanov, T. A. Sjöström, D. T. Simon, M. Berggren, G. G. Malliaras, C. Bernard, *Adv. Mater.* **2015**, *27*, 3138.

[13] E. Stavrinidou, R. Gabrielsson, K. P. R. Nilsson, S. Kumar, J. F. Franco-gonzalez, A. V Volkov, M. P. Jonsson, A. Grimoldi, M. Elgland, I. V Zozoulenko, D. T. Simon, M. Berggren, *Proc. Natl. Acad. Sci.* **2017**, *114*, 2807.

[14] C. B. Nielsen, A. Giovannitti, D. T. Sbircea, E. Bandiello, M. R. Niazi, D. A. Hanifi, M. Sessolo, A. Amassian, G. G. Malliaras, J. Rivnay, I. McCulloch, *J. Am. Chem. Soc.* **2016**,

138, 10252.

[15] A. Giovannitti, D.-T. Sbircea, S. Inal, C. B. Nielsen, E. Bandiello, D. A. Hanifi, M. Sessolo, G. G. Malliaras, I. McCulloch, J. Rivnay, *Proc. Natl. Acad. Sci.* **2016**, *113*, 12017.

[16] C. Cendra, A. Giovannitti, A. Savva, V. Venkatraman, I. McCulloch, A. Salleo, S. Inal, J. Rivnay, *Adv. Funct. Mater.* **2019**, *29*, 1807034.

[17] L. Q. Flagg, C. G. Bischak, J. W. Onorato, R. B. Rashid, C. K. Luscombe, D. S. Ginger, *J. Am. Chem. Soc.* **2019**, *141*, 4345.

[18] S. Inal, G. G. Malliaras, J. Rivnay, *Nat. Commun.* **2017**, *8*, 1767.

[19] Y. Yuan, G. Giri, A. L. Ayzner, A. P. Zoombelt, S. C. B. Mannsfeld, J. Chen, D. Nordlund, M. F. Toney, J. Huang, Z. Bao, *Nat. Commun.* **2014**, *5*, 3005.

[20] H. U. Khan, J. Jang, J.-J. Kim, W. Knoll, *J. Am. Chem. Soc.* **2011**, *133*, 2170.

[21] J. Huang, J. Miragliotta, A. Becknell, H. E. Katz, *J. Am. Chem. Soc.* **2007**, *129*, 9366.

[22] L. Torsi, G. M. Farinola, F. Marinelli, M. C. Tanese, O. H. Omar, L. Valli, F. Babudri, F. Palmisano, P. G. Zambonin, F. Naso, *Nat. Mater.* **2008**, *7*, 412.

[23] M. Mushrush, A. Facchetti, M. Lefenfeld, H. E. Katz, T. J. Marks, *J. Am. Chem. Soc.* **2003**, *125*, 9414.

[24] A. Borghese, G. Geldhof, L. Antoine, *Tetrahedron Lett.* **2006**, *47*, 9249.

[25] J. R. Reynolds, K. J. Barth, L. R. Savagian, A. M. Österholm, J. F. Ponder, J. Rivnay, *Adv. Mater.* **2018**, *30*, 1804647.

[26] J. Heinze, B. A. Frontana-Uribe, S. Ludwigs, *Chem. Rev.* **2010**, *110*, 4724.

[27] S. Goffri, C. Müller, N. Stingelin-Stutzmann, D. W. Breiby, C. P. Radano, J. W. Andreasen, R. Thompson, R. a J. Janssen, M. M. Nielsen, P. Smith, H. Sirringhaus, *Nat. Mater.* **2006**, *5*, 950.

[28] L. H. Jimison, A. Hama, X. Strakosas, V. Armel, D. Khodagholy, E. Ismailova, G. G. Malliaras, B. Winther-Jensen, R. M. Owens, *J. Mater. Chem.* **2012**, *22*, 19498.

[29] A. J. Bard, L. R. Faulkner, *Electrochemical Methods: Fundamentals and Applications*,

Wiley, New York, NY, USA **2001**.

[30] A. Savva, R. Hallani, C. Cendra, J. Surgailis, T. C. Hidalgo, S. Wustoni, R. Sheelamanthula, X. Chen, M. Kirkus, A. Giovannitti, A. Salleo, I. McCulloch, S. Inal, *Adv. Funct. Mater.* **2020**, *1907657*..

[31] C. B. Nielsen, A. Angerhofer, K. A. Abboud, J. R. Reynolds, *J. Am. Chem. Soc.* **2008**, *130*, 9734.

[32] K. J. Thorley, I. McCulloch, *J. Mater. Chem. C* **2018**, *6*, 12413.

[33] C. G. Bischak, L. Q. Flagg, K. Yan, C.-Z. Li, D. S. Ginger, *ACS Appl. Mater. Interfaces* **2019**, *11*, 28138.

[34] Z. S. Parr, R. Halaksa, P. A. Finn, R. B. Rashid, A. Kovalenko, M. Weiter, J. Rivnay, J. Krajčovič, C. B. Nielsen, *ChemPlusChem* **2019**, *84*, 1384.

[35] A. Giovannitti, C. B. Nielsen, D. T. Sbircea, S. Inal, M. Donahue, M. R. Niazi, D. A. Hanifi, A. Amassian, G. G. Malliaras, J. Rivnay, I. McCulloch, *Nat. Commun.* **2016**, *7*, 13066.

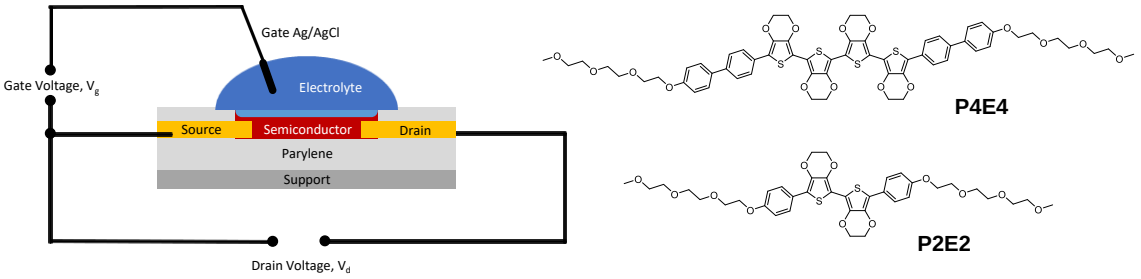

Figure 1. Schematic illustration of an organic electrochemical transistor together with the molecules **P2E2** and **P4E4** studied in this work.

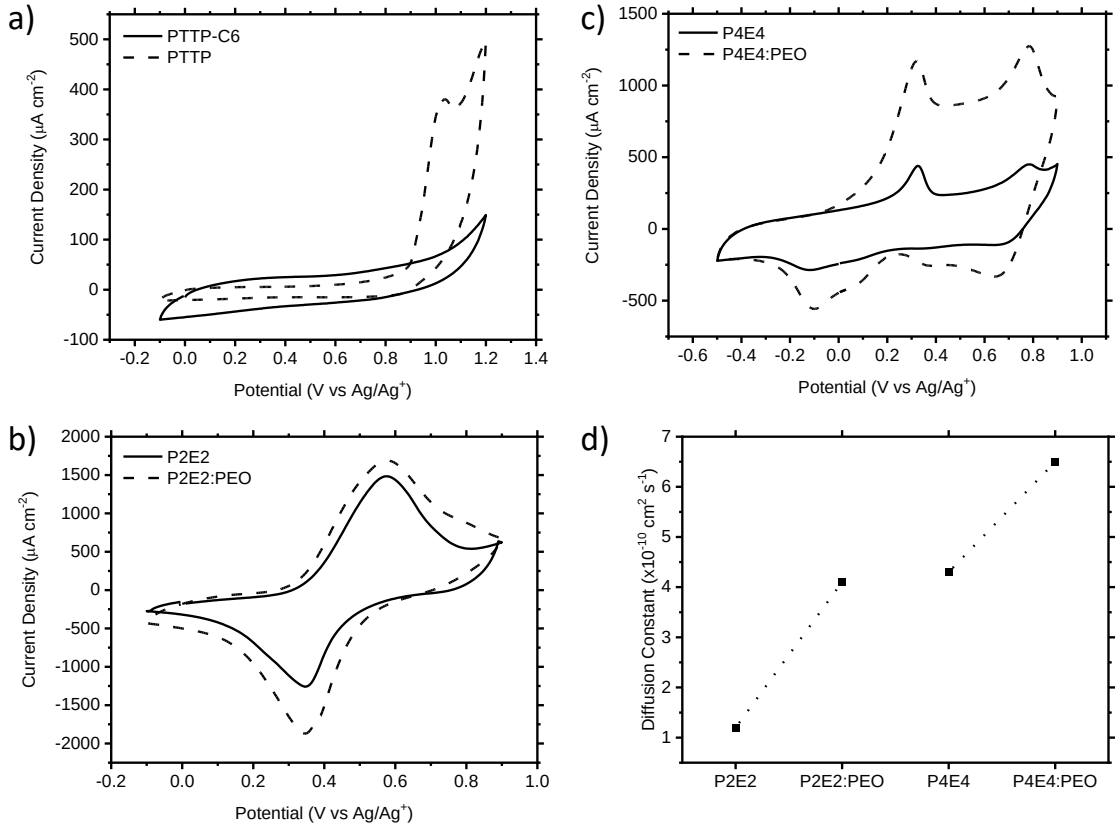

Figure 2. Thin film cyclic voltammetry of neat molecule and molecule:PEO blend films drop-cast onto a glassy carbon electrode from 5 mg/mL chloroform solutions. Cyclic voltammograms recorded at 100 mv/s in 0.1 M aqueous NaCl supporting electrolyte after two cycles apart from **PTTP** for which we report the first cycle. (a) **PTTP-C$_6$** and **PTTP** (b) **P2E2** and **P2E2**:PEO (c) **P4E4** and **P4E4**:PEO. (d) Diffusion coefficients for molecule and molecule:PEO blends.

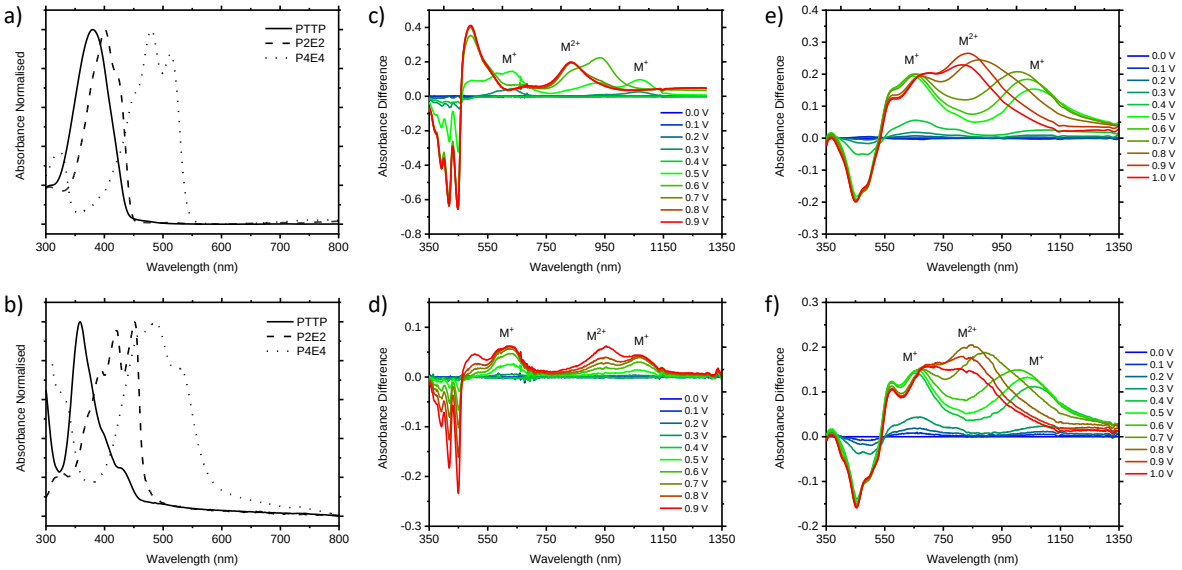

Figure 3. Optical characterisation of small molecules; (a) solution phase UV-Vis spectra of molecules at 1×10^{-5} M in DCM; (b) solid state UV-Vis spectra of thin films spin-coated onto glass slides from 5 mg/mL chloroform solutions. Thin film spectroelectrochemistry in 0.1 M NaCl supporting electrolyte of (c) **P2E2**, (d) **P2E2**:PEO, (e) **P4E4**, and (f) **P4E4**:PEO plotted as absorption difference for clarity.

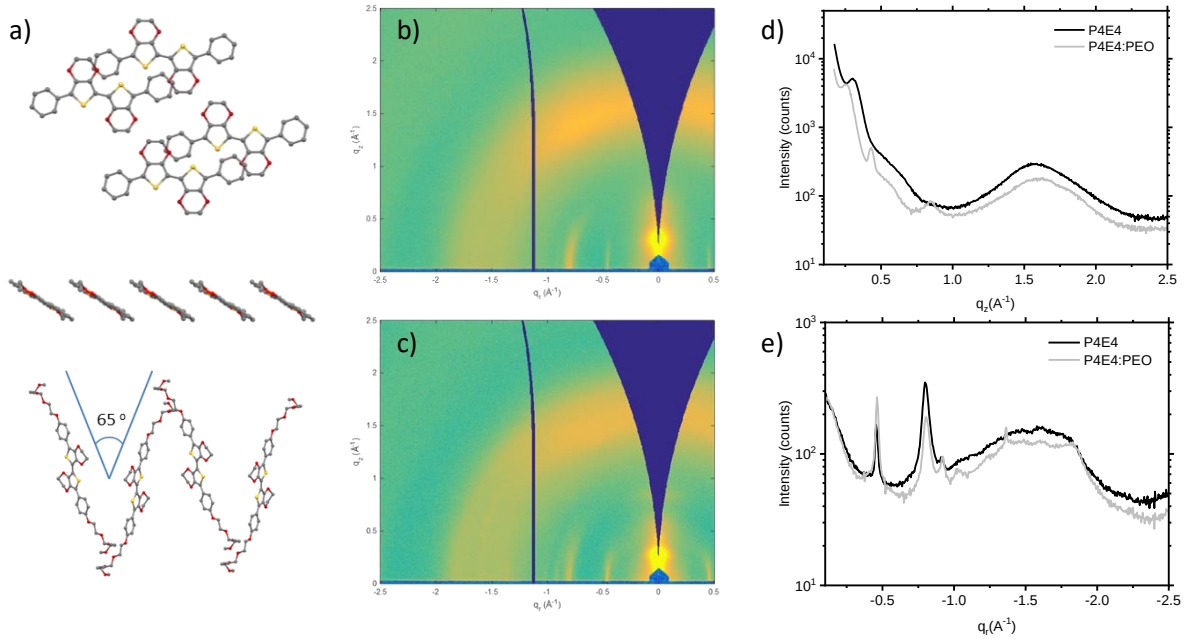

Figure 4. (a) Crystal structure of **P2E2** illustrating packing perpendicular to plane of **P2E2** molecule, showing offset (top); side view of packing of molecules (middle), and packing depicting angled arrangement of layers (bottom). GIWAXS data for (b) **P4E4** neat film and (c) **P4E4**:PEO, both spin-coated from chloroform; (d) out-of-plane q_Z line cuts, and (e) in-plane q_r line cuts for **P4E4** neat and **P4E4**:PEO blend films.

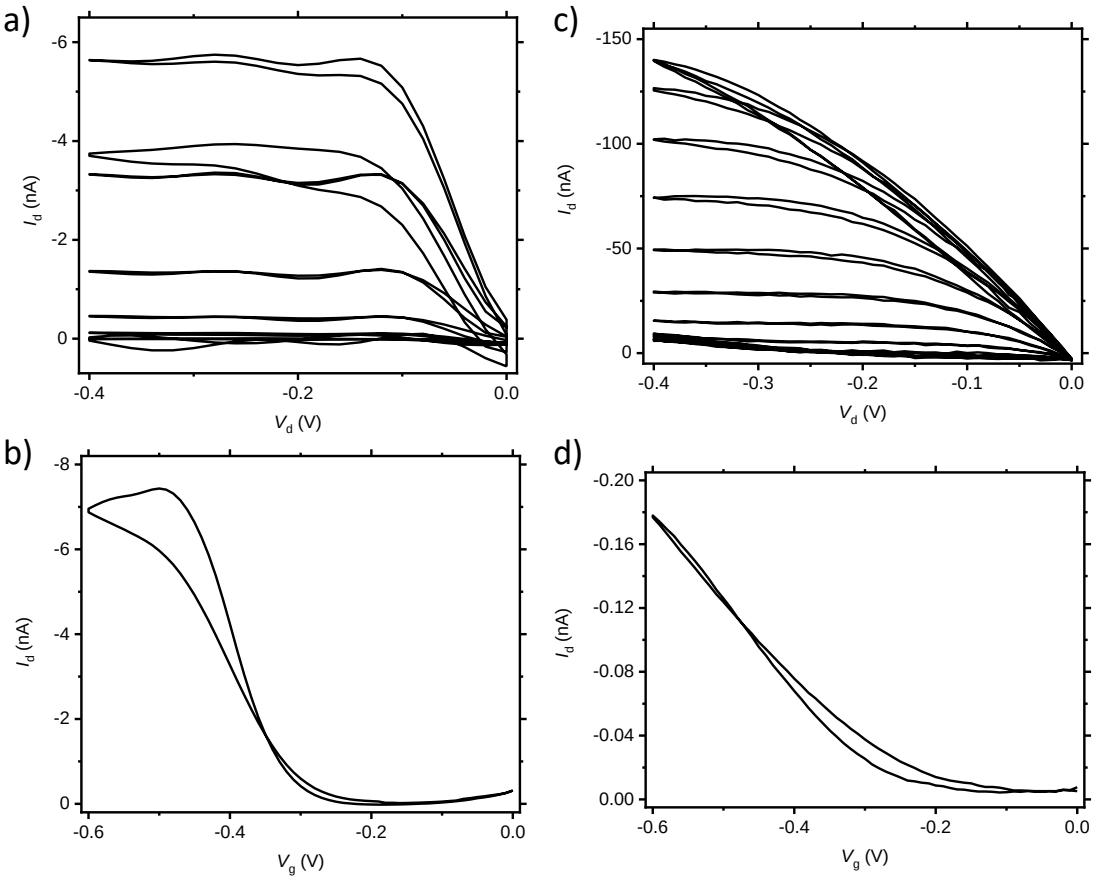

Figure 5. Output and transfer curves for OECTs with neat molecules and their blends. OECT dimensions 10×10×100 μm. (a) Output and (b) transfer curve for **P2E2**:PEO. (c) Output and (d) transfer curves for **P4E4**:PEO. Output curves at 50 mV gate potential steps, at a sweep rate of 0.05 Vg/s, transfer curves recorded with V_d of – 0.4 V.

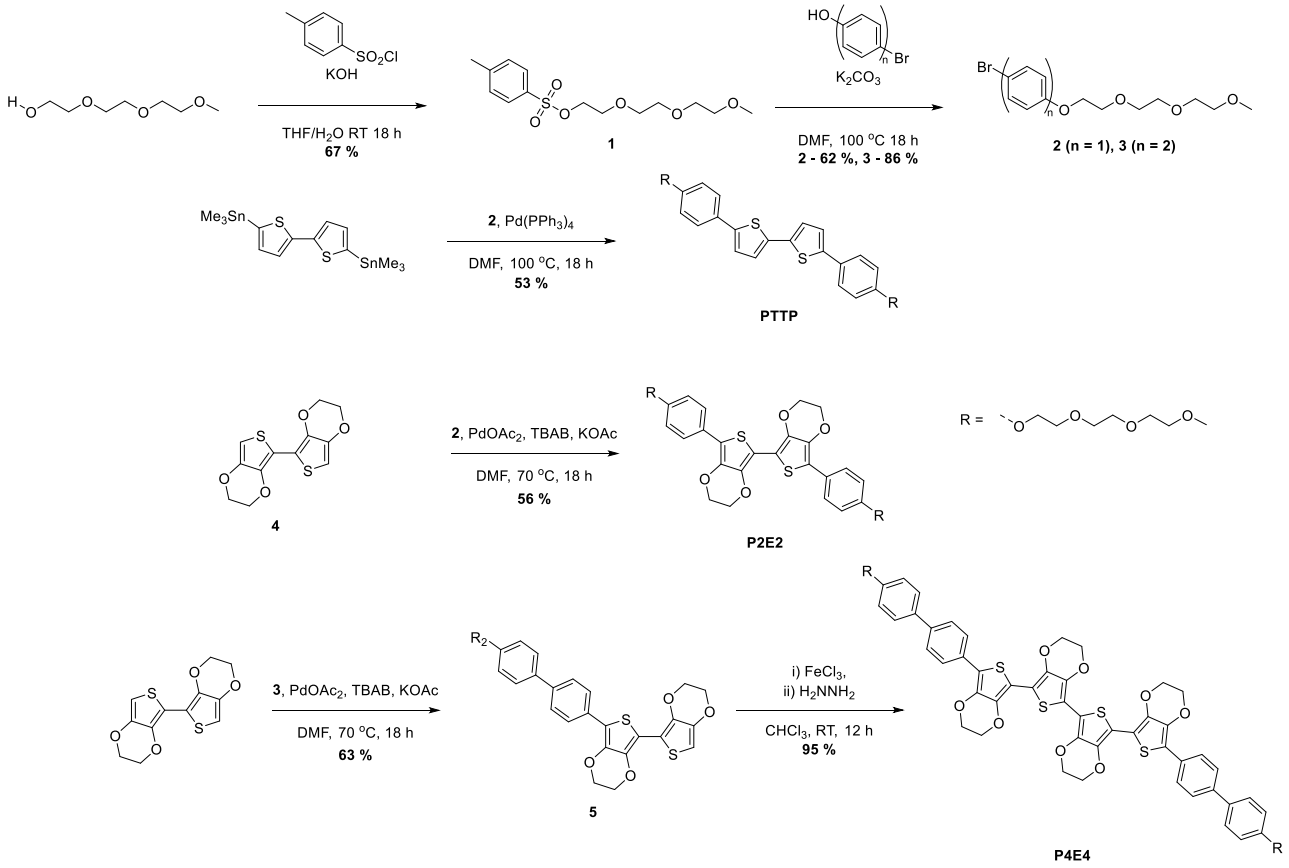

Scheme 1. Synthetic scheme for the molecules **PTTP**, **P2E2** and **P4E4**.

Table 1. Summarized electrochemical properties.

	$E_{1/2}^{(1)}$ [V][a)]	$E_{1/2}^{(2)}$ [V][a)]	$E_{1/2}^{film}$ [V][b)]	E_{ox}^{film} [V][b)]
PTTP-C_6	0.51	1.01	-	-
PTTP	0.39	0.72	0.97*	0.93*
P2E2	0.04	0.50	0.46	0.34
P4E4	0.01	0.23	0.10	0.22

a) Solution half-wave potentials measured for 0.001 M solutions in DCM with 0.1 M $TBAPF_6$ supporting electrolyte versus Fc/Fc^+ with Pt wire counter electrode and glassy carbon working electrode; b) Films drop cast onto glassy carbon electrode with 0.1 M NaCl supporting electrolyte versus Ag/Ag^+ reference electrode; *Values reported for first cycle; all other values reported for second cycle.